Available online at www.sciencedirect.com
SCIENCE DIRECT®
Journal of Power Sources 124 (2003) 40–46
JOURNAL OF POWER SOURCES
www.elsevier.com/locate/jpowsour

Fabrication of miniature silicon wafer fuel cells with improved performance

Jingrong Yu [a,b], Ping Cheng [a,*], Zhiqi Ma [a], Baolian Yi [b]

[a] *Department of Mechanical Engineering, Hong Kong University of Science and Technology, Clear Water Bay, Kowloon, Hong Kong*
[b] *Fuel Cell R&D Center, Dalian Institute of Chemical Physics, Chinese Academy of Sciences, Dalian 116023, PR China*

Received 19 December 2002; received in revised form 11 April 2003; accepted 21 May 2003

Abstract

The fabrication and performance evaluation of miniature fuel cells on silicon wafers are presented in this paper. The miniature fuel cells consisted of a membrane–electrode-assembly (MEA) between two silicon substrates. The feed holes and channels in the silicon wafers, acting as a fuel distributor, were prepared by anisotropic silicon etching from the back and front of the wafer using silicon dioxide as an etching mask. In an attempt to reduce the cell resistance and consequently improving cell performance of the miniature silicon wafer fuel cell, a Cu/Au composite layer was sputtered on the top of silicon wafers as a current collector. Testing results show that (i) the cell performance was improved by increasing the thickness of the composite layer on the silicon wafer, and (ii) the miniature silicon wafer fuel cell with smaller size channels gave a better performance at the diffusion-limiting current region.

Keywords: Proton exchange membrane fuel cell; Miniature fuel cell; Micro-fabrication; Silicon wafer; Cu/Au current collector

1. Introduction

Proton exchange membrane (PEM) fuel cells have been considered to be a promising technology for renewable energy systems such as an alternative battery for stationary and portable applications [1–6]. Conventional proton exchange membrane fuel cell designs have been based on the structure that uses machined or pressure-moulded plates as the current collector and fuel distributor [7]. These plates are usually made of graphite, carbon-polymer composites or metals that are rather bulky in size [8]. In the past several years, much attention has been given to the use of micro-electronic fabrication technology for the fabrication of miniature fuel cells using silicon wafers as the polar plate of fuel cells [9–14]. The advantages of micro-electronic fabrication technology include fine feature resolution, high repeatability, batch operation, integrated process sequences, and a variety of material transfer options [14,15]. For application as a micro-power source, miniature fuel cells must have small volumes and small mass and their performance should approach or exceed that of large systems in order to be competitive. It has been reported that the cell performance of these miniature fuel cells using silicon wafer as a current collector is lower than those of conventional fuel cells [9–14]. In a recent paper, Meyers and Maynard [10] suggested that the high cell resistance may be one of the major reasons for the low cell performance of these minature fuel cells. Therefore, much effort is needed to reduce the cell resistance in order to improve the performance of miniature fuel cells.

The objective of this paper is to fabricate miniature silicon wafer fuel cells using a Cu/Au composite layer as the current collector to reduce cell resistance, and consequently improving its cell performance. Effects of the Cu/Au composite layer thickness on the cell performance and resistance were evaluated in a single cell test fixture. A comparison of performance between the miniature silicon wafer fuel cell with smaller size channels and a standard fuel cell (using the same membrane–electrode-assembly, MEA) with graphite polar plates having larger size channels is also presented.

2. Experimental

2.1. Fabrication of miniature fuel cells on silicon wafer

In this section, we describe the fabrication of a miniature fuel cell using a silicon wafer as the polar plate, which was made by micro-fabrication techniques. The silicon wafer was prepared following a series of micro-electronic fabrication steps similar to those discussed by Kelley et al. [11,12],

* Corresponding author. Tel.: +852-2358-7181; fax: +852-2358-1543.
E-mail address: mepcheng@ust.hk (P. Cheng).

0378-7753/$ – see front matter © 2003 Elsevier Science B.V. All rights reserved.
doi:10.1016/S0378-7753(03)00618-9

Sim et al. [13] and Madou [15]. The original material was a 525 ± 25 μm-thick p-type ⟨1 0 0⟩ silicon wafer with resistivity ranging from 15 to 25 Ω cm. The first step was to deposit silicon dioxide layer on the wafer for Si etching mask. To make feed holes, the silicon dioxide on the back-side of the wafer was patterned by photolithography. Dry etching was first applied on silicon dioxide of the back-side wafer, and then the exposed surface of silicon was etched with tetra-methylammonium hydroxide (TMAH) solution at about 90 °C. To align the micro-channels with feed holes, a photolithography machine with infrared ray was employed. The silicon dioxide on the front-side of the wafer was patterned, and the front-side wafer was etched using the same processes mentioned above to fabricate the channels. Subsequently, silicon dioxide was deposited on the entire surface of the silicon wafer again. This step was to ensure that no fresh silicon surface was exposed in the channels and holes so that the metal layer would be bonded well in contact with the silicon wafer. Finally, a layer of Au or Cu/Au (acting as a current collector) was sputtered on the front-side of the silicon wafer with titanium/tungsten layer as adhesive.

The membrane–electrode-assembly components used in this system are similar to those typically used in proton exchange membrane fuel cells [16,17]. The pre-treatment of Nafion membranes was performed by the following four sequential boiling steps: in 3% H_2O_2 solution, in deionized water, in 0.5 M H_2SO_4 solution, and in deionized water, each of the above step lasted for 1 h. Twenty percent Pt/C catalyst, carbon paper, PTFE suspension, and a Nafion solution (Aldrich, 5 wt.% in 15–20% water/low aliphatic alcohol) were used for electrode preparation. The catalyst layer (Pt loading of 0.4 mg/cm^2) of the electrodes was impregnated with the Nafion solution with dry Nafion loading of 1.0 mg/cm^2. Two electrodes with effective area of 5 cm^2 (22.5 mm × 22.5 mm) were hot-pressed to one piece of Nafion112 membrane at 135 °C and 10 MPa to form the membrane–electrode-assembly (MEA). Four MEAs with the same structure were used in this experiment. Then, it was clamped mechanically onto a glass cell for performance evaluation. A schematic diagram on the structure of the miniature fuel cell is shown in Fig. 1. It should be noted that the current generated by the MEA is conducted from the two lateral electrical contact pads, shown as components 4 and 8 in Fig. 1. The miniature twin-fuel-cell was installed in an Arbin fuel cell test station.

2.2. Cell performance evaluation

To evaluate cell performance, pure hydrogen and oxygen without any humidification were used as fuel and oxidant under atmospheric pressure. The fuel cell was operated at the room temperature of 25 °C. The flow rates of H_2 and O_2 were controlled both at 50.0 ml/min. Before collecting data, the cell was allowed to equilibrate for 48 h at a current density of 100 mA/cm^2. The discharge of the fuel cell was controlled with an electric load system (BT2000, Arbin Instrument Inc.). To measure the cell resistance, the response of the cell voltage was continuously monitored and recorded when the fuel cell was applied with a discharge current pulse of fast drop time. The software of BT 2000 automatically calculated the differential resistance approximately according to a cell voltage change (ΔE) divided by a current change (Δi) during the fast drop time.

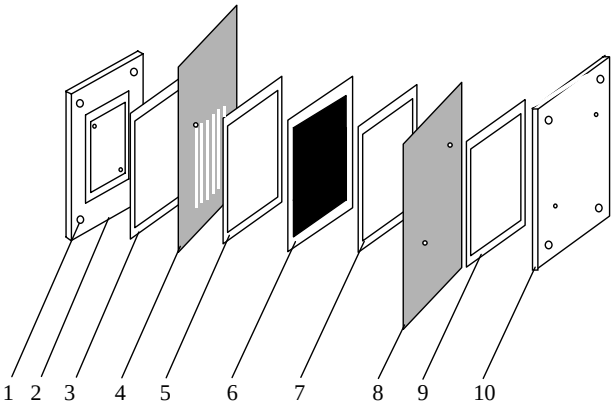

Fig. 1. Schematic diagram of the structure of the miniature fuel cell. (1) Tighten holes; (2, 10) end plates; (3, 5, 7, 9) seal gaskets; (4, 8) silicon wafers; (6) membrane–electrode-assembly.

3. Results and discussion

Cross-sectional SEM micrographs of the various thickness of the current collector on the top of silicon wafer are presented in Fig. 2a–c, respectively. As shown in these figures, the thicknesses and materials of the current collectors were: (a) 0.5 μm Au, (b) 1.4 μm Cu and 0.2 μm Au, (c) 1.5 μm Cu and 0.9 μm Au, respectively. The cells fabricated with above-mentioned silicon wafers are denoted as Cells #1–3 in Table 1, which had the same polar plate material, the same channel shape and dimension, the same MEA, the same cell active area except that the material and thickness of the composite layer were different. Fig. 3 presents the cell potential versus current density characteristics of Cells #1–3 operating at 25 °C and 0.10/0.10 MPa of dry H_2/O_2. The shape of potential versus current density curve is typical for a PEM fuel cell. The initial drop of the polarization curve at very low current density was due to an electrochemical activating process, which was caused by the sluggish kinetics of oxygen reduction at the cathode surface. The subsequent linear decrease of the polarization curve was due to ohmic over-potential, which was attributed to the ion flow through the electrolyte membrane, the electron flow through the electrode materials and current collector. The voltage drop at high current density was due to the mass transport limitations occurring in the electrodes and in the membrane. As shown in Fig. 3, the thickness of current collector on the top of silicon wafer plays an important role in cell performance. The thicker the current collector, the better is the cell performance. For example, at 0.4 V (the low

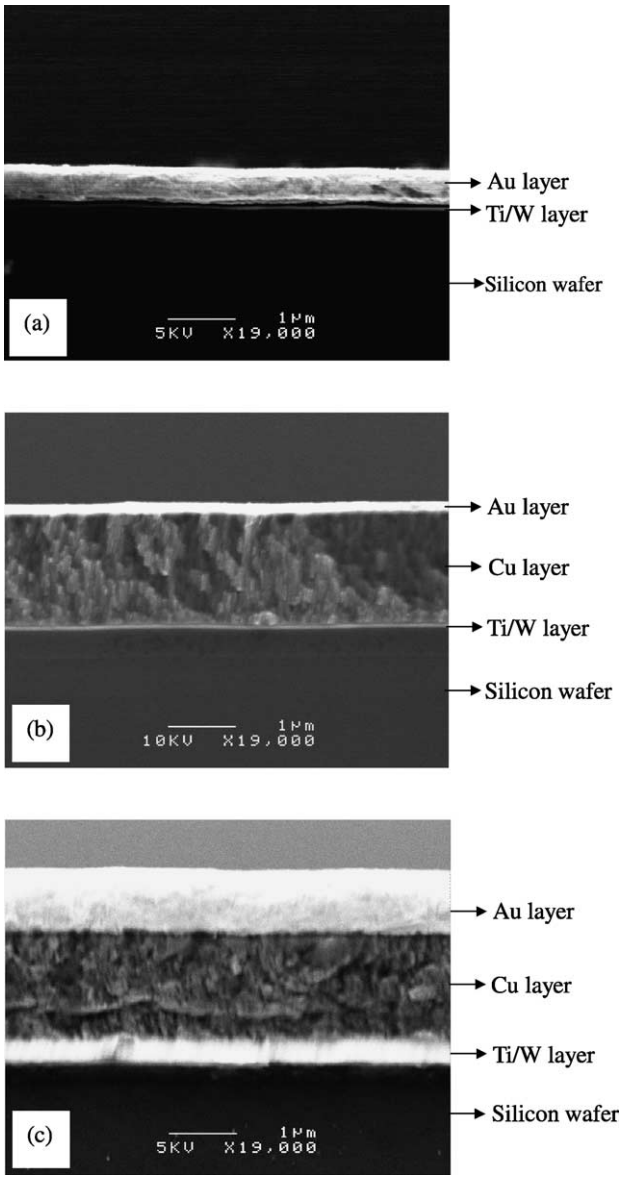

Fig. 2. Cross-sectional SEM micrographs of various thickness of current collector on the top of silicon wafer. (a) 0.5 μm Au; (b) 1.4 μm Cu and 0.2 μm Au; (c) 1.5 μm Cu and 0.9 μm Au.

voltage of the polarization curves) the current densities of Cells #1–3 were 270, 385 and 480 mA/cm^2, respectively. This improvement in cell performance was because the cell resistance was reduced by increasing the current collector thickness, which is revealed by the resistance curves measured during acquisition of the polarization curves (Fig. 3). The "*iR*-corrected" polarization curves can be obtained by adding the ohmic losses across the current collector to the cell potential curves in Fig. 3. Such "*iR*-corrected" polarization curves for the Cells #1–3 are presented in Fig. 4. It is shown that performance of the three cells is almost the same after the differences in current collector resistance are accounted for. In the present miniature silicon wafer fuel cells, current generated by the MEA was conducted from the lateral electrical contact pads to the outside circuit. Therefore, the process of increasing the current collector thickness will increase the area of conductor, which decreases the cell resistance and consequently improving the cell performance. This improved performance by increasing the thickness of the current collector can also be seen from the power density versus current density curves presented in Fig. 5. It can be seen from this figure that the peak power density of the Cells #1–3 were 107.3 (at 260 mA/cm^2), 155.3 (at 380 mA/cm^2) and 194.3 mW/cm^2 (at 450 mA/cm^2), respectively.

To the best of our knowledge, the idea of sputtering a Cu/Au composite layer on the top of the silicon wafer acting as a current collector has not been done before. There are three reasons for choosing Cu/Au composite material as the current collector. Firstly, using Cu instead of Au will reduce the production cost. Secondly, the use of Cu can overcome some problems caused by micro-fabrication technology. For example, the Au layer is easily to be peeled off from the silicon wafer when its thickness exceeds 0.5 μm. This can be seen from Fig. 2a, where the Au layer is obviously separated from the silicon wafer. Finally, the resistivity of Cu (1.673 μΩ cm at 20 °C) is lower than that of Au (2.350 μΩ cm at 20 °C) [18].

We now turn our attention to the comparison of experimental results of the miniature silicon wafer fuel cell (Cell #3) with those of Electrochem. Inc., fuel cell (denoted as Cell #4 in Table 1), which has been commonly used to evaluate

Table 1
Characteristics of cells tested

	Cell #1	Cell #2	Cell #3	Cell #4
Polar plate material	Au on silicon wafer	Cu/Au on silicon wafer	Cu/Au on silicon wafer	Graphite
Thickness of current collector	0.5 μm Au	1.4 μm Cu & 0.2 μm Au	1.5 μm Cu & 0.9 μm Au	
Channel arrangement	Three-pass serpentine			
Channel shape and cross-section area	Trapezoid (top width:bottom width:height = 409.2:107.8:207.7 μm), 0.0537 mm^2			Square (width:height = 0.7:0.7 mm), 0.49 mm^2
Components of MEA	Anode: carbon paper as diffuser, 0.4 mg Pt/cm^2 at catalyst layer Electrolyte: Nafion112 membrane Cathode: the same as the anode			
Cell active area	5 cm^2 (22.5 mm × 22.5 mm)			
Cell operating conditions	Cell temperature at 25 °C, dry H_2/O_2 gas pressure at 0.10/0.10 MPa, gas flow rate of H_2/O_2 at 50/50 ml/min			

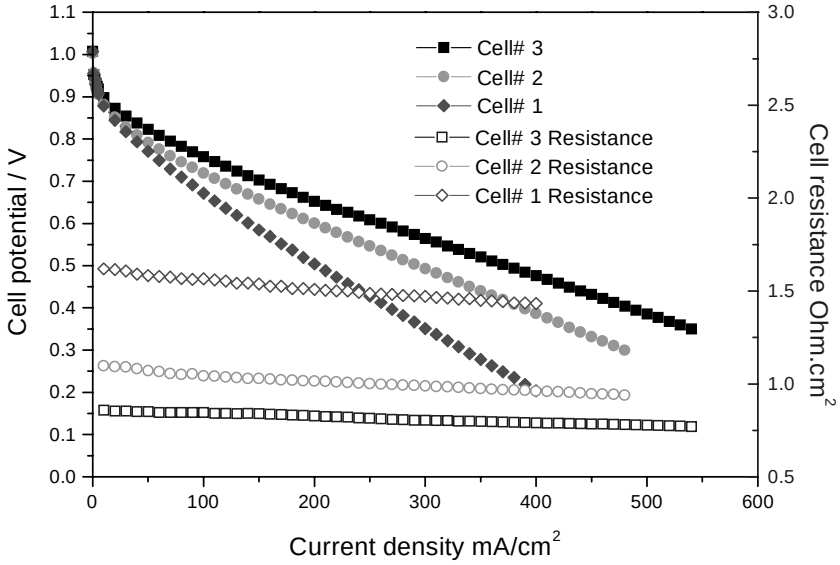

Fig. 3. Polarization and resistance curves of Cells #1–3, respectively: cell temperature at 25 °C, dry H_2/O_2 gas pressure at 0.10/0.10 MPa, gas flow rate of H_2/O_2 at 50/50 ml/min.

cell performance in the published literature [19]. As shown in Table 1, Cells #3 and #4 had the same MEA, the same cell active area and the same three-pass serpentine. The only differences were the shape and the size of the channels and the materials used as the polar plate. Cell #3 had a cross-sectional area of 0.0537 mm^2 while Cell #4 had a cross-sectional area of 0.49 mm^2. Thus, the channel size of Cell #3 is therefore 1/9 of that of Cell #4.

A comparison of polarization and cell resistance of Cells #3 and #4 is shown in Figs. 6 and 7, respectively. Fig. 6 shows that the performance of Cell #3 is similar to those of Cell #4 at the low and intermediate current densities. The performance of Cell #3 is much higher than that of Cell #4 at high current densities. Fig. 6 also shows that the resistance of Cell #3 is slightly higher than that of Cell #4 over the whole range of current density, with the difference ranging from 0.07 to 0.10 $\Omega\,cm^2$. As can be clearly seen in Fig. 7, the polarization of Cell #3 with smaller size channels on silicon wafers maintains its linear variation up to 500 mA/cm^2, while the polarization of Cell #4 with graphite plates having larger size channels departs greatly from the linear behavior when the current density is greater than 300 mA/cm^2. This drop from linearity can be attributed to the concentration over-potential. In this region, the potential loss is mainly due to mass transport limitations [20]. The concentration over-potential will happen when the chemical reaction is limited by the rate at which the reactants can be supplied. The lack of reactants will slow down the electrochemical

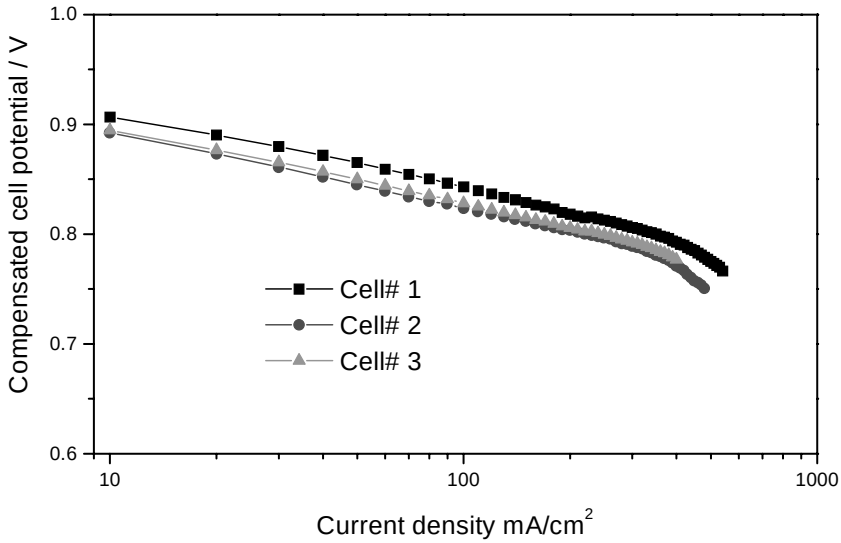

Fig. 4. *iR*-corrected performance curves of Cells #1–3, respectively: the operating conditions of the cells are the same as those in Fig. 3.

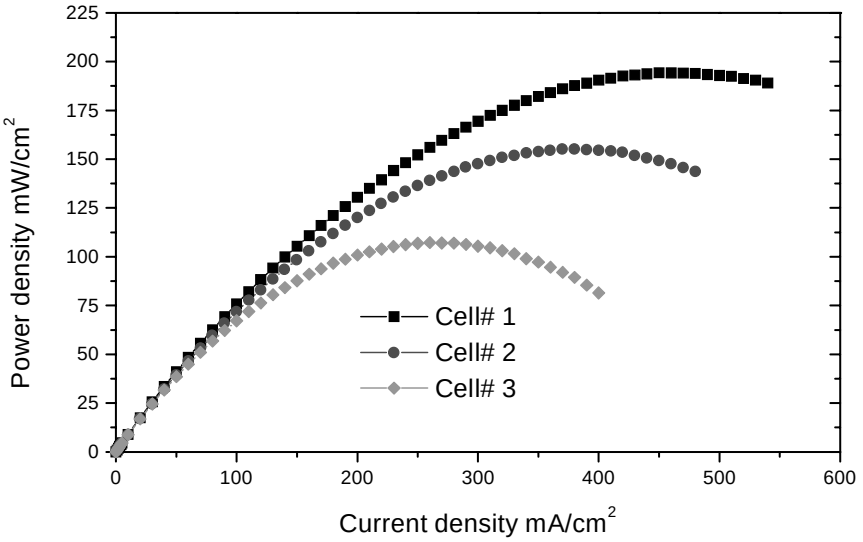

Fig. 5. Power density vs. current density curves of Cells #1–3, respectively: the operating conditions of the cells are the same as those in Fig. 3.

reaction, leading to a decrease in cell potential. It is well known that current density is directly proportional to the reaction rate. At high current density, the mass transport of reactants and products of the electrochemical reaction becomes the dominant limitation to cell potential. This can be explained by considering the electrochemical reaction at the cathode:

$$2H^+ + \frac{1}{2}O_2 + 2e^- = H_2O \quad (1)$$

where the mass transport process of reactant proton depends on the membrane thickness while the removal of water depends on the structure of the electrode under the same gas flow rate of the cells. It is shown from Fig. 7 that there is no mass transport limitation occurring in Cell #3. Since Cells #3 and #4 have the same MEA structure and cell operating conditions, the proton transport and the water removal rate have no effect on the drop of cell potential. Thus, the drop in potential cell in Cell #4 must be originated from the oxygen transport process due to its slower velocity in the channel. This is apparent because the flow rate of reactant was the same at 50 ml/min in both cells but the channel size of Cell #3 is 1/9 of that of Cell #4, the gas flow velocity in channel of Cell #3 is more than nine times higher than that of Cell #4. Because of the low viscosity of H_2 and O_2, there were very small pressure drops (in comparison of the ambient pressure) between the inlet and outlet in Cells #3 and #4. Thus, the gas pressures in both cells were at the ambient condition.

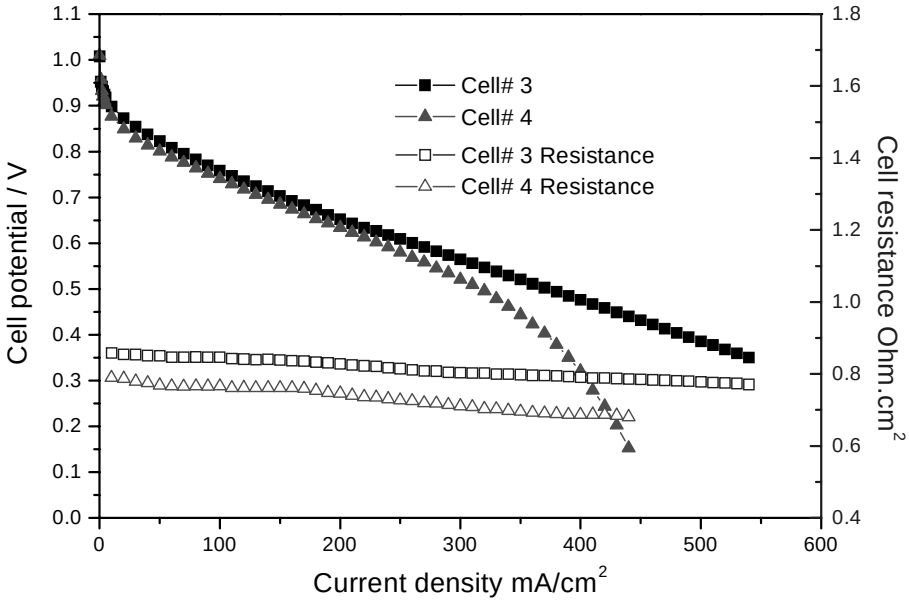

Fig. 6. Polarization and resistance curves of Cells #3 and #4, respectively: the operating conditions of the cells are the same as those in Fig. 3.

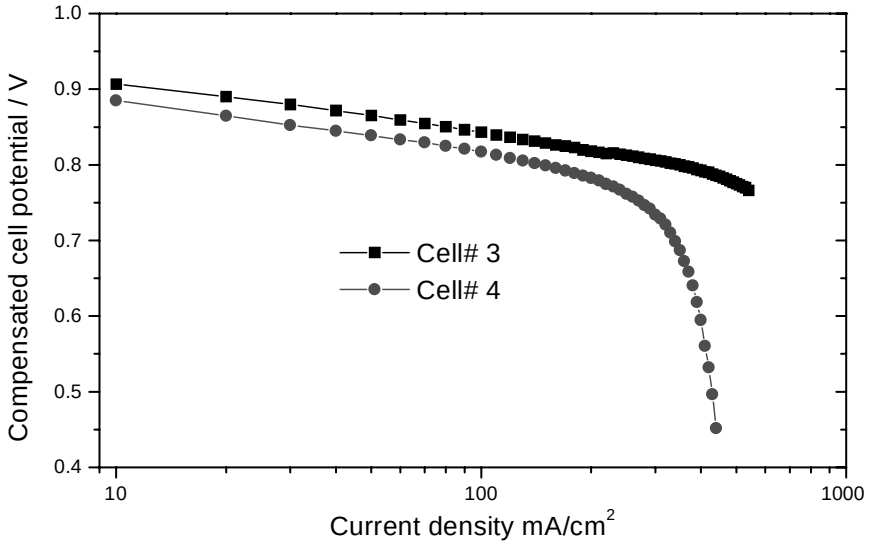

Fig. 7. *iR*-corrected performance curves of Cells #3 and #4, respectively: the operating conditions of the cells are the same as those in Fig. 3.

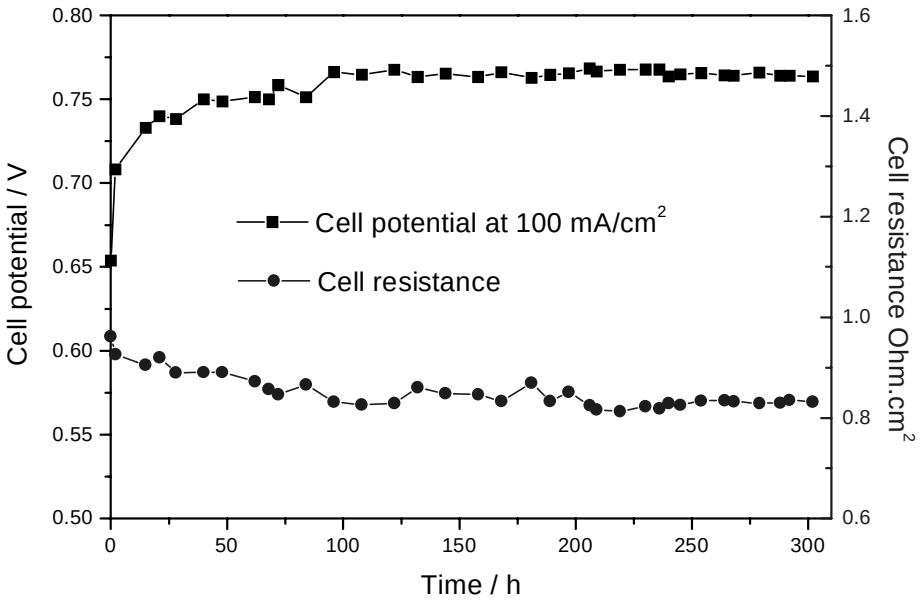

Fig. 8. Long-term testing of cell performance and resistance vs. time for Cell #3: the operating conditions of the cell are the same as those in Fig. 3.

In order to determine the stability behavior of the silicon wafer fuel cell with the Cu/Au composite layer sputtered as the current collector, Cell #3 was selected for long-term stability assessment. The potential versus time measurements were recorded for 300 h at 100 mA/cm^2 under ambient conditions. During the 300 h, some measurements of the cell potential versus the current density were taken. The results are presented in Fig. 8, where the potential and resistance versus time of the miniature fuel cell with H_2/O_2 is shown. The cell was operated at a current density of 100 mA/cm^2, and the potential was improved from 0.654 to 0.760 V after 100 h of operation. One reason for this improvement might be that the organic impurities in the cell components were removed by the oxidation reaction at the electrodes. Another possibility was that the hydration state of the electrolyte membrane became higher. Also, the active regions in the catalyst layer were enlarged after 100 h operation [21]. Subsequently, the potential was constant at approximately 0.760 V. The bonding between the electrode and the membrane appeared to be excellent, and no cracking or delamination was observed after completing the lifetime test. The experimental results show that using the micro-electronic fabrication technique to fabricate a miniature fuel cell on silicon wafers is promising for practical applications.

4. Concluding remarks

In this paper, a miniature fuel cell on silicon wafers has been successfully fabricated using micro-electronic

fabrication techniques including photolithography, dry and wet etching, chemical and physical vapor deposition. It is found sputtering a Cu/Au composite layer on the top of the silicon wafer can reduce its resistance as a current collector. Test results indicate that the cell performance is improved by increasing the thickness of the composite layer on the silicon wafer. Furthermore, the miniature silicon wafer fuel cell with smaller size channels gave better performance than the state-of-the-art fuel cell with larger size channels at the diffusion-limiting current region.

Acknowledgements

The authors would like to acknowledge that this work was supported by the grants HKUST6014/02E as well as HIA 98/99.EG04.

References

[1] E.A. Ticianelli, C.R. Derouin, S. Srinivasan, J. Electroanal. Chem. 251 (1988) 175.
[2] A.J. Appleby, Phil. Trans. R. Soc. Lond. A 354 (1996) 1681.
[3] B.C.H. Steele, A. Heinzel, Nature 414 (2001) 345.
[4] A. Heinzel, C. Hebling, M. Muller, M. Zedda, C. Muller, J. Power Sources 105 (2002) 250.
[5] G. Cacciola, V. Antonucci, S. Freni, J. Power Sources 100 (2001) 67.
[6] C.K. Dyer, J. Power Sources 106 (2002) 31.
[7] W.R. Merida, G. Mclean, N. Djilali, J. Power Sources 102 (2001) 178.
[8] D.R. Hodgson, B. May, P.L. Adcock, D.P. Davies, J. Power Sources 96 (2001) 233.
[9] L. Mex, N. Ponath, J. Muller, Fuel Cells Bull. 39 (2002) 9.
[10] J.P. Meyers, H.L. Maynard, J. Power Sources 109 (2002) 76.
[11] S.C. Kelley, G.A. Deluga, W.H. Smyrl, AICHE J. 48 (2002) 1071.
[12] S.C. Kelley, G.A. Deluga, W.H. Smyrl, Electrochem. Solid State Lett. 3 (2000) 407.
[13] W.Y. Sim, G.Y. Kim, S.S. Yang, IEEE Int. Conf. Micro Electro. Mech. Sys, 14th ed., 2001, p. 341.
[14] S.J. Lee, A. Chang-Chien, S.W. Cha, R. O'Hayer, Y.I. Park, Y. Saito, F.B. Prinz, J. Power Sources 112 (2002) 410.
[15] M. Madou, Fundamentals of Microfabrication, CRC Press, Boca Raton, FL, 1997.
[16] X. Du, J. Yu, B. Yi, M. Han, K. Bi, Phys. Chem. Chem. Phys. 3 (2001) 3175.
[17] X. Chen, B. Yi, M. Han, J. Zhang, Y. Qiao, J. Yu, J. Power Sources 79 (1999) 75.
[18] D.L. Perry, S.L. Phillips, Handbook of Inorganic Compounds, CRC Press, Boca Raton, FL, 1995.
[19] C. Lim, C.Y. Wang, J. Power Sources 113 (2003) 145.
[20] Y.W. Rho, O.A. Velev, S. Srinivasan, Y.T. Kho, J. Electrochem. Soc. 141 (1996) 2084.
[21] Z. Qi, A. Kaufman, J. Power Sources 111 (2002) 181.